DOI: 10.15587/978-617-7319-97-8.CH4

Anatoliy Narivskiy, Oleg Shinsky, Inna Shalevska,
Yuliia Kvasnitska, Pavlo Kaliuzhnyi, Svitlana Polyvoda

CHAPTER 4

THE INFLUENCE OF EXTERNAL ACTIONS AND METHODS OF ALLOYING ALLOYS ON THE OPERATIONAL CHARACTERISTICS OF CAST PRODUCTS

ABSTRACT

The chapter presents the results of scientific research on the influence of electromagnetic stirring and alloying on the properties of deformable aluminum alloys, the influence of alloying elements on the phase state and structural stability of heat-resistant corrosion-resistant alloys, which are used for the manufacture of turbine blades of gas turbine engines (GTE), is analyzed. The results of studies on the effect of alloying a heat-resistant nickel-based alloy with tantalum and rhenium on its operational characteristics are presented.

The influence of excess pressure on the properties and quality of castings from iron-carbon alloys during lost foam casting is determined.

It is determined that under the controlled influence of technological factors and excess pressure (2...6 MPa) on liquid metal and during its crystallization, it is possible to increase the mechanical strength and reduce the porosity of cast iron and steel castings by 15...30 %, compared to gravity casting according to models, which are gasified.

The latest technological processes for the production of ordinary and reinforced castings with specified properties by casting according to gasified models, using excess pressure on the metal, have been developed.

The work carried out by the authors at the Physical and Technological Institute of Metals and Alloys of the National Academy of Sciences of Ukraine is of high scientific and practical importance for the production of high-quality foundry products and will be useful for foundry product manufacturers, scientific and scientific-pedagogical workers of the specialty "Metallurgy" (Foundry production).

KEYWORDS

Deformable aluminum alloys, vacuum magnetohydrodynamic complex, heat-resistant alloy, gas turbine engine, turbine blade, continuously cast aluminum ingots, modification, iron-carbon alloys, lost foam casting, thermal destruction of polystyrene, physical and mechanical properties of cast structures, influence of pressure on metal.

The high quality of structural materials can be ensured by using the latest methods of preparing alloys, based on the intensification of the processes of interaction of gas, liquid and solid phases with the melt. The use of plasma, centrifugal and electromagnetic actions on metal systems in a vacuum provides wide opportunities for the creation of effective technologies for mass and special purpose metal production, based on the processes of treating alloys with dispersed and active reagents in a highly reactive state. The creation of such breakthrough technologies for obtaining high-quality structural materials with economical consumption of energy resources and materials is relevant and meets the requirements of science and practice at the current stage.

To achieve greater efficiency of gas turbines in the fields of aviation power and ship gas turbine construction, an important task is to increase the operating temperatures at the turbine inlet. However, different types of turbines are designed to work on different types of fuel and in different operating conditions. Therefore, there is a need to use heat-resistant nickel alloys with different chemical compositions and physical properties to meet the specifications and requirements of different turbines in these industries. The relevance and economic significance of research is due to the intensive development of unique technology and the growing need for materials with increased or new functional characteristics.

In order to achieve the guaranteed quality and strength of cast structures due to the increase in the mechanical properties of iron-carbon alloys, the effect of regulated pressure on the metal in the mold during lost foam casting was investigated.

4.1 MODERN PROCESSES OF PRODUCTION OF CAST STRUCTURAL MATERIALS FROM ALUMINUM ALLOYS FOR PRODUCTS OF RESPONSIBLE PURPOSE

4.1.1 THE INFLUENCE OF EXTERNAL ACTIONS AND MELT ALLOYING METHODS ON THE STRUCTURES AND PROPERTIES OF PRODUCTS MADE OF DEFORMABLE ALUMINUM ALLOYS

Deformable aluminum alloys with a unique complex of mechanical and operational properties have low density, sufficiently high strength and machinability, are an irreplaceable structural material for the aerospace, automotive and shipbuilding industries, as well as for the production of special military equipment.

Many years of experience have established a direct dependence of the mechanical and technological properties of ingots on their primary structure, which is formed in the process of crystallization during continuous casting. Ingots with a uniform fine-crystalline (non-dendritic) structure have the highest properties, which ensures:

– 1.5–2.0 times increase in plasticity in the cast state with high resistance to cracking of ingots;

– reduction by 2–3 times of the duration of homogenizing annealing of ingots before plastic deformation;

– a 4–6-fold reduction in the pressing force of semi-finished products and an increase in crack resistance during hot deformation;

– 20–30 % increase in strength and 1.3–1.8 times the plasticity of products made from these ingots compared to semi-finished products with a dendritic structure.

The structure in ingots is dispersed by modifying alloys with manganese, chromium, zirconium, scandium and other elements. The primary structure in ingots is crushed also when ultrasonic, electromagnetic, vibrational vibrations and other external influences are applied to the liquid metal.

The Physics and Technology Institute of Metals and Alloys of the National Academy of Sciences of Ukraine has developed and successfully operates a melting and pouring complex, which includes a vacuum magnetodynamic mixer (MHD-mixer) and a continuous ingot casting machine (CICM) [1] (**Fig. 4.1**). The use of such a complex for the preparation of aluminum alloys and the continuous casting of ingots from them allows [2]:

– constantly stir the liquid metal with electromagnetic forces during the preparation of alloys. Due to this, increase the degree of assimilation of alloying elements by the melt and evenly distribute them in cast products;

– refine the alloy in a vacuum (dilution ~1 mm Hg) with constant electromagnetic stirring of the alloy and reduce the hydrogen content in the ingots to 0.05–0.12 cm^3/100 g of metal;

– pass the melt through a ceramic filter and effectively remove oxide inclusions until their final concentration in the alloy is ≤0.05 vol. %;

– create a protective atmosphere of inert gases above the melt in the MHD unit and during feeding into the crystallizer, which excludes additional gas saturation and oxidation of the alloy;

– regulate the intensity of electromagnetic mixing of the alloy in the crystallizer and control the process of structure formation in ingots.

Most deformable aluminum alloys, especially high-strength ones, contain refractory elements Mn, Cr, Ti, Zr, etc. As a rule, ligatures are used for their introduction into the alloy. One of the main advantages of preparing aluminum alloys in a vacuum MHD mixer is the intensification of the dissolution processes of elements, including pure refractory metals. Their dissolution occurs in the active zone – the section of the mixer channel, where the magnetic fields of the inductor and the electromagnet interact, thus creating the maximum magnetohydrodynamic factors of influence on the melt [3]. So, for example, it was shown [4] that with the optimal combination of the magnitude and direction of action of volumetric electromagnetic forces in the active zone of the MHD mixer, pure chromium in the amount of 3.0 wt. % can be dissolved in aluminum in ~20 minutes without significantly overheating the metal.

The properties of deformable aluminum alloys are largely determined by their hydrogen content, the presence of which leads to the development of macro- and microporosity, prevents the welding of discontinuities formed during pressure treatment. The influence of vacuum refining of the melt in the MHD mixer on the quality of continuous cast ingots from the secondary aluminum alloy AD31 [5] is shown on the example of experimental melts, the technological regimes of which are given in **Table 4.1**. The quality of ingots from the AD31 alloy must meet the requirements of the standards of regulatory documentation.

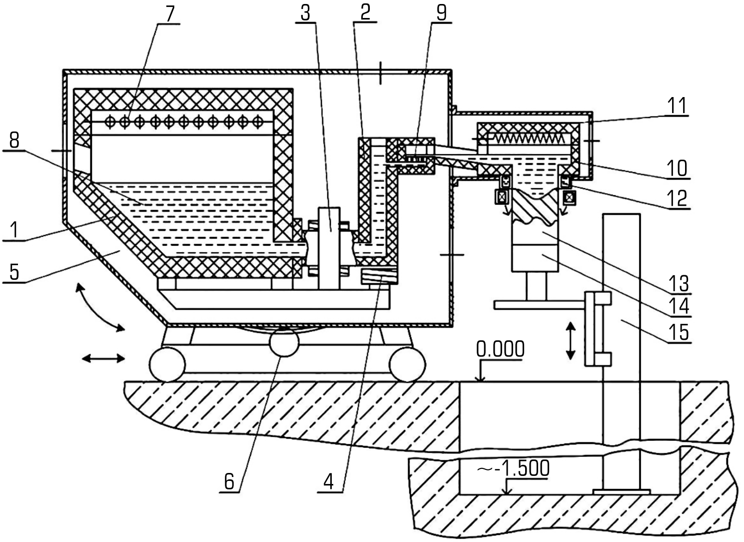

1 – crucible;
2 – metal conduit;
3 – inductor;
4 – electromagnet;
5 – vacuum chamber;
6 – vacuum chamber rotation drive;
7 – heating elements;
8 – liquid metal;
9 – camera with foam ceramic filter;
10 – thermal nozzle;
11 – filling device;
12 – crystallizer;
13 – ingot;
14 – seed;
15 – mechanism of vertical movement of the crystallizer

Fig. 4.1 Vacuum MHD complex for the preparation of aluminum alloys and continuous casting of ingots from them

Table 4.1 Technological parameters of the preparation of secondary alloy AD31 and continuous casting of ingots from it

Melting No.	Melting of the charge on the "dry floor"	Overflow to the MHD-mixer through the KS11LA filter mesh	Modification with Al-Ti-B ligature	Modes of vacuum refining		Filtration through a porous ceramic filter	Ingot casting modes	
				Vacuum, mm Hg	Refining duration		Temperature, °C	Casting speed, mm/min
1	+	+	–	–	–	+	690–705	110
2	+	+	+	–	–	+	690–705	110
3	+	+	+	1	30	+	690–705	110

It can be seen that in ingots made of alloys without melt processing in a vacuum (melts No. 1, 2), the hydrogen content is 0.4–0.5 cm^3/100 g of metal, which exceeds the requirements of regulatory documentation (≤0.3 cm^3/100 g). The concentration of hydrogen in vacuum metal ingots (melt No. 3) is 0.05–0.07 cm^3/100 g.

The macrostructure of the ingots (melts No. 1 and No. 2) is coarse-grained fan-shaped with a clear arrangement of dendrites in the radial direction (**Fig. 4.2, *a***).

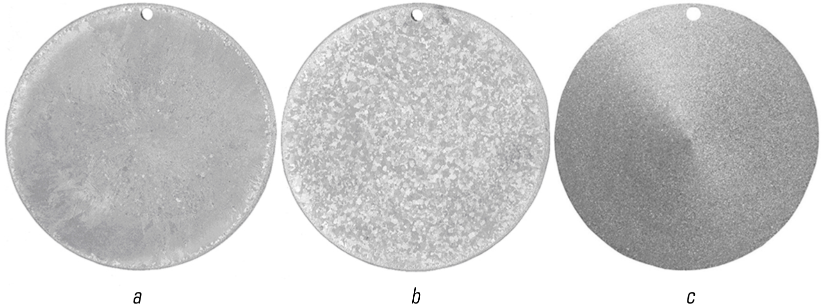

Fig. 4.2 Macrostructure of experimental ingots from secondary alloy AD31: *a* – melt No. 1; *b* – melt No. 2; *c* – melt No. 3

Alternating zones of fan-shaped and coarse-grained equiaxed structures, as well as light veins and non-metallic inclusions are also observed (**Fig. 4.2, *b***). The macrostructure of the ingots (melt No. 3) obtained from the vacuum-refined alloy is fine-grained, homogeneous, without light spots and non-metallic inclusions (**Fig. 4.2, *c***) and fully meets the requirements of the standards. In this way, vacuum refining makes it possible to obtain ingots from the secondary AD31 alloy, which in terms of their properties are at the level of cast metal made from primary materials.

During the vacuum refining of high-strength aluminum alloys, one of the main alloying elements – zinc – evaporates, the content of which can reach ~10 %. To eliminate the evaporation of zinc, the rarefaction above the alloy in the vacuum chamber must be higher than the value of its vapor elasticity. Thus, in industrial technologies for the preparation of such alloys with vacuum treatment in a ladle or mixer, the rarefaction above the melt during refining is maintained at a level of ≥10 mm Hg. With such a vacuum, a lot of hydrogen remains in the ingots after crystallization (0.27–0.29 cm^3/100 g of metal). For the preparation of high-strength aluminum alloys with a high zinc content in a vacuum MHD unit, a technology has been developed that allows eliminating losses of this alloying element by evaporation and reducing the hydrogen content in ingots to 0.05 cm^3/100 g of metal [6].

For the preparation of high-quality aluminum alloys, a refining method was developed [7] using successive vacuum pulses, which ensures a residual concentration of hydrogen in ingots at the level of 0.01–0.03 cm^3/100 g of metal. Methods of operational control of the hydrogen content in liquid metal [8] were also created, which made it possible to automate the process of preparing alloys in the MHD-unit.

The quality and properties of ingots made of deformable aluminum alloys significantly depend on the concentration of oxide inclusions, in particular, Al_2O_3 in them. To eliminate (reduce) oxidation of the liquid metal, all components of the vacuum MHD complex (mixer crucible, dispensing chamber and crystallizer) are hermetically connected. Such a connection allows creating a protective environment of inert gases over the metal at all stages of ingot production from melting to casting. The creation of a protective environment is especially relevant when preparing alloys that contain easily oxidizable elements, for example, magnesium (alloys 1560, 1575, 1545, etc.).

The oxide film formed on the surface of aluminum alloys of the Al-Mg system during their melting has low strength and is destroyed when the liquid metal is stirred. Therefore, during the preparation of alloys with magnesium, the surface film does not protect the melt from oxidation. To protect such alloys from oxidation, small beryllium additives are introduced into the melt, which form a dense film of beryllium-magnesium oxides on the surface of the liquid metal bath. Such a film significantly reduces the oxidation of alloys and the content of non-metallic inclusions in ingots. However, beryllium and its compounds are poisonous, and its use in the production of alloys is dangerous. Therefore, the task of excluding beryllium from the technologies of preparing alloys of the Al-Mg system is urgent. The effectiveness of using a protective argon environment against metal oxidation in the production of ingots from the experimental alloy 1545 containing 4.5 % by mass. magnesium, shown in **Table 4.2**. It can be seen that the ingots (melt No. 1), obtained without protection of the melt from oxidation, have a tensile strength of 30 %, and the relative elongation is 2.4 times less than that of ingots from an alloy that protected against oxidation (melts No. 2 and No. 3).

Table 4.2 Conditions for experimental melting of alloy 1545 and results of mechanical tests of samples in the cast state

Melting No.	Melting peculiarities	Mechanical properties		
		$\sigma_{0.2}$, MPa	σ_B, MPa	δ, %
1	Without the use of measures to protect the melt from oxidation	132	215	5
2	With the use of a ligature Al-5 wt. % Be (based on 0.0003 wt. % Be in the alloy)	204	294	12
3	With the use of protective argon environment	207	292	13

An important factor affecting the crystallizing metal is electromagnetic stirring. To regulate the intensity of mixing of the alloy during the crystallization of the ingot, a low crystallizer with a thermal nozzle and an electromagnetic stirrer is installed on the continuous casting machine (**Fig. 4.3**). The design of the crystallizer is designed so that the magnetic field of the stirrer affects the alloy in the liquid and liquid-solid state.

With the help of electromagnetic stirring, it is possible to influence the nature and speed of movement of liquid metal in the crystallizer [9]. In order to exclude bubbling in the crystallizer and tightening of oxide films from the alloy surface into the middle of the ingot, the melt movement should be laminar (value $Re<6900$). If this indicator is exceeded, the quality of the ingot deteriorates and liquid metal may break through the surface layer of the ingot, which has begun to crystallize.

The use of electromagnetic stirring during continuous casting also allows for the alignment of the crystallization front of the alloy, which helps to reduce the anisotropy of properties and internal stresses in the ingot. At the same time, the structural components in the alloy are crushed. Mixing is advisable when introducing modifiers into the melt, which intensifies the process of nucleation in the alloy and contributes to the uniform distribution of crystallization centers near the solidification front of the ingot. The movement of liquid metal in the crystallizer during electromagnetic stirring is shown in **Fig. 4.3**.

The effectiveness of the influence of electromagnetic stirring of the B96C alloy during its crystallization on the structure of a continuously cast ingot with a diameter of 90 mm is shown in **Fig. 4.4**. The part of the ingot produced without electromagnetic stirring of the alloy during the casting process (**Fig. 4.4**, upper part) has an uneven coarse crystal structure with a micrograin size ~350 microns. The ingot part that was cast using electromagnetic stirring has a uniform fine crystal structure with a micrograin size of ~100 μm (**Fig. 4.4**, lower part).

The positive effect of electromagnetic mixing of the alloy in the ingot during its crystallization can be shown on the example of the production of a ligature bar Al–2.5 % by mass. Zr with an improved structure for modifying alloys directly in the crystallizer of a continuous casting machine [10].

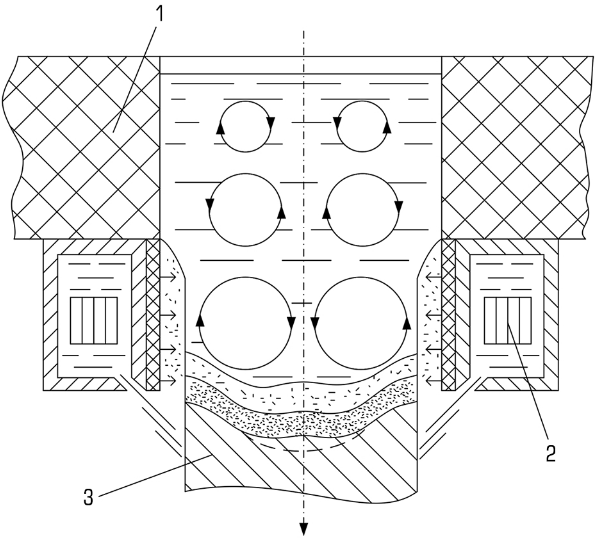

Fig. 4.3 Scheme of liquid metal movement during electromagnetic stirring in the crystallizer

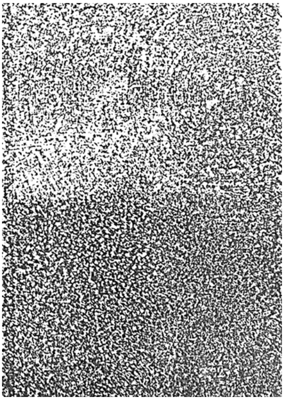

Fig. 4.4 Macrostructure of the longitudinal section of a continuously cast ingot ∅90 mm from the B96Ts alloy: the upper part – without electromagnetic stirring; the lower one – with electromagnetic stirring of the alloy in the ingot

Technology of preparation of ligature alloy Al–2.5 % by mass. Zr from primary materials (aluminum grade A85 and zirconium grade KTC) consists in dissolving crushed zirconium in aluminum in the active zone of the MHD mixer at a temperature of 820 °C, followed by its increase to 1000 °C and exposure for 20 minutes. To avoid oxidation of the alloy, melting was carried out in a protective argon atmosphere. A continuously cast ingot with a diameter of 50 mm was produced. One part of the ingot was obtained without electromagnetic stirring of the alloy, the second – with stirring at an electromagnetic stirrer current of 160 A.

Part of the ingot of the ligature alloy, made without electromagnetic stirring, contains large (up to 100 μm) acicular Al_3Zr intermetallics, which reduce the mechanical properties of the alloy. Part of the ingot made with electromagnetic mixing of the alloy contains a modifying phase of 3–10 μm. Thus, the use of electromagnetic mixing of the alloy during ingot crystallization allows the structure to be dispersed in aluminum ligatures containing various refractory elements.

The modifying ability of the ligature bar Al–2.5 wt. % Zr and the influence of its modification of the alloy in the crystallizer on the mechanical properties of ingots were determined on the B96C1 alloy. The alloy was prepared in a vacuum MHD mixer from primary materials. The zirconium content in the alloy was 0.10 wt. %. Two ingots of ∅150 mm were cast from the prepared alloy. The first of them was obtained by continuous modification of the alloy in the crystallizer with a ligature rod Al–2.5 wt. % Zr. This rod was produced by continuous casting with electromagnetic stirring of the ligature during the crystallization process. With the help of a rod, an additional 0.03 wt. was introduced into the alloy. % of zirconium. After dissolving the rod, the total concentration of zirconium in the alloy was ~0.13 % by mass.

After casting the first ingot into the alloy remaining in the MHD mixer, crushed zirconium was added to its content in the alloy ~0.13 wt. % and produced a second ingot using the usual technology without bar modification. The structures of the experimental ingots are shown in **Fig. 4.5**. The average grain size in the ingot obtained by conventional technology is ~280 μm, and in the ingot from an alloy modified with a ligature rod – ~80 μm. After the homogenization annealing of the ingots, pressing and heat treatment according to the standard regimes for the B96C1 alloy, samples for mechanical tests were made, the results of which are presented in **Table 4.3**.

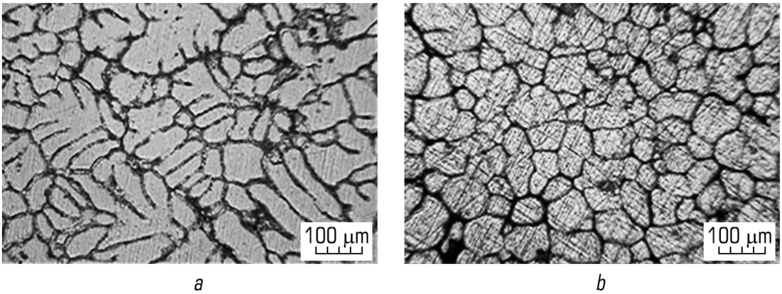

Fig. 4.5 Microstructure of continuously cast ingots with a diameter of 150 mm from the B96Ts1 alloy: *a* – produced according to traditional technology; *b* – modified with a ligature bar Al–2.5 % by wt. Zr

Table 4.3 Mechanical properties of hot-pressed billets from the B96C1 alloy

Manufacturing technology	σ_B, **MPa**	$\sigma_{0.2}$, **MPa**	δ, **%**
Modification with a ligature bar Al–2.5 % by mass. Gold	669	642	7.2
Traditional	632	611	4.5

It can be seen that after continuous modification with a rod made of ligature Al–2.5 % wt. Zr obtained using electromagnetic mixing of the alloy in the crystallizer, the grain size in the ingots decreases by 3.5 times, the tensile strength and yield strength (σ_B, $\sigma_{0.2}$) of the pressed products increases by 5–6 %, the relative elongation – by 35–40 % compared to experimental blanks made from an alloy that was modified according to traditional technology.

The created melting and pouring MHD equipment can be combined with plasmatrons and develop effective processes for preparing alloys and obtaining cast products from them [11, 12]. An example of such technologies can be the method of plasma nitriding of aluminum alloys in the MHD mixer (**Fig. 4.6**).

The high-strength aluminum alloy B93pch was melted in a mixer. The first ingot with a diameter of 250 mm was obtained from the prepared alloy by continuous casting. In the melt that remained in the mixer after the production of the first ingot, a ligature of Al–5 % by mass was introduced. Ti based on the calculation of the titanium content in the alloy ~0.05 % by mass. Then, the titanium-doped alloy was treated with a plasma nitrogen jet immersed in the liquid metal. Nitriding of the alloy was carried out for 1.5–2 min at a voltage on the plasmatron of 60...65 V, a constant current of 380÷400 A, and a nitrogen consumption of ~7.5 l/min. After plasma nitriding of the melt, the B93pch+Ti+PN alloy was obtained, which was further refined in a vacuum and a second ingot with a diameter of 250 mm was cast from it.

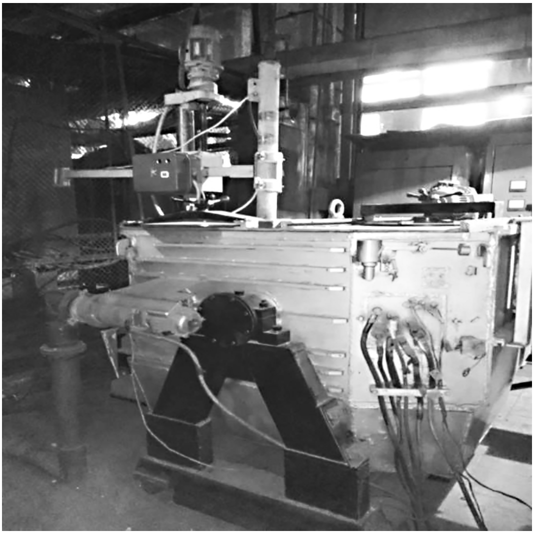

Fig. 4.6 Vacuum MHD mixer with plasmatron

It was determined that the first Ingot from the B93pch alloy has a dendritic heterogeneous structure. The average grain size in it is 25÷30 % larger than in a cast made of a plasma-nitrided alloy (**Fig. 4.7, *a***). In an alloy ingot doped with titanium and nitride by plasma, the structure is dispersed with a uniform distribution of grains of the same size (**Fig. 4.7, *b***).

After the homogenization annealing of the ingots, isothermal pressing and heat treatment of the pressed products were carried out according to the T1 mode. The mechanical properties of the samples of the obtained products are shown in **Table 4.4**. It can be seen that after alloying with titanium and MHD-plasma nitriding of the alloy, the mechanical properties of pressed parts from continuously cast ingots increase: the tensile strength and yield strength (σ_B, $\sigma_{0.2}$) increase by 7÷10 %, relative elongation – by 20÷25 % compared to the requirements of OST 1 90073-85 for stampings made of alloy B93pch.

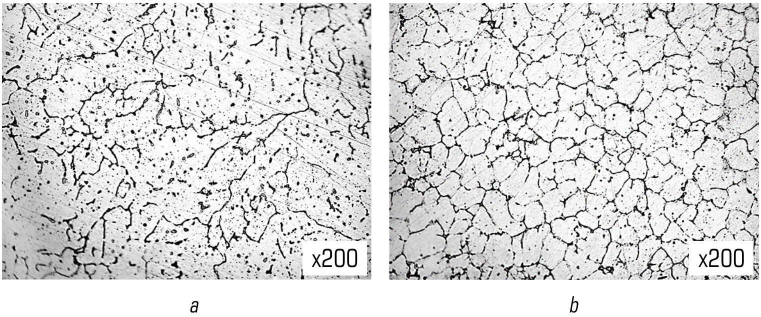

a *b*

Fig. 4.7 Microstructure of continuously cast ingots with a diameter of 250 mm from experimental alloys: *a* – B93pch; *b* – B93pch+Ti+PN

Table 4.4 Mechanical properties of products from experimental alloys

Alloy	**Mechanical properties**		
	σ_B, **MPa**	$\sigma_{0.2}$, **MPa**	δ, **%**
B93pch	486	447	6.9
B93pc+Ti+PN	517	472	7.3
Requirements of OST 1 90073-85 for stampings from alloy V93pch	480	440	6.0

It is advisable to use the results of the performed research at enterprises that produce metal products of responsible and special purpose from aluminum alloys, as well as at foundry and metallurgical mini-plants.

4.2 INFLUENCE OF ALLOYING ELEMENTS ON SPECIAL PROPERTIES OF HEAT-RESISTANT ALLOYS

The problem of the resistance of marine gas turbine materials to high-temperature salt corrosion (HSC) is critical, especially compared to aircraft turbines that operate on refined kerosene, a light fuel, where HSC is not a problem. To ensure resistance to HSC, it is often necessary to increase the chromium content in materials, but this can lead to a decrease in the strength of alloys at high temperatures. In the case of aircraft alloys, the chromium content is usually limited to 6–8 wt. %, which is not feasible for alloys used in marine gas turbines. This creates an actual problem, since the temperature of the working environment in aircraft turbines is higher than in marine ones, and increasing this temperature becomes such an important task [13–15]. Unlike air turbines, marine turbines operate on heavy fuel with a high content of sulfur and other harmful impurities, as well as in the presence of water vapor and sea salts, which contribute to HSC.

The problem of creating multi-component heat-resistant nickel-based alloys for the blades of stationary gas turbine units (GTU) requires improving the structural and phase stability of materials. This improvement contributes to the reliability of the materials during long-term operation, which can be from 50 to 100 thousand hours at a temperature from 750 to 950 °C. It is especially important to achieve this stability under conditions of exposure to fuel with aggressive sulfur and vanadium impurities, which can affect the material.

The results of the assessment of the strength and durability of the main components and parts of the stationary gas turbine engine indicate the need to improve the operational characteristics of the working blades of the 1st and 2nd stages of the gas turbine. **Table 4.5** shows the chemical composition of modern global heat-resistant alloys for high-pressure gas turbine blades.

Heat-resistant corrosion-resistant alloys such as IN792 and CMSX-4 are known for their structural stability due to the balanced content of elements such as tantalum (Ta), molybdenum (Mo) and tungsten (W) (**Table 4.5**) [16, 17]. However, despite this stability, these alloys show insufficient long-term strength and corrosion resistance at the average surface temperature of the blades, which is up to 850 °C.

According to literature data [18–20], rhenium and tantalum are elements that exhibit the properties of effective hardeners of austenitic solid solution (rhenium) and active carbide and γ'-phase formers (tantalum). This helps to increase the heat resistance of the alloy. The structural stability of alloys containing rhenium and tantalum with the appropriate chromium content and the presence of topologically densely packed phases (TDPP-phases) will be determined both by the total content of refractory elements and their mutual ratio.

Table 4.5 Chemical composition of modern global heat-resistant alloys for high-pressure turbine blades of gas turbines

Alloy brand	**Cr**	**Ni**	**Co**	**Mo**	**Re**	**W**	**Al**	**Ti**	**Ta**	**Nb**	**Hf**
IN 738LC	16.0	base	8.5	1.7	–	2.6	3.4	3.4	3.4	0.9	–
CMSX-11C	14.9	base	3.0	0.4	–	4.5	3.4	4.2	5.0	0.1	0.04
SC PWA 1483	12.8	base	9.0	1.9	–	3.8	3.6	4.1	5.0	–	–
Rene 80H	14.1	base	9.2	4.0	–	4.0	3.1	4.7	–	–	0.74
DC GTD 111	14.0	base	9.5	1.5	–	3.8	3.0	4.9	2.8	–	0.15
CMSX-4	6.5	base	9.6	0.6	3.0	6.4	5.6	1.0	6.5	–	0.10
CM88Y	15.9	base	11.0	1.9	–	5.3	3.05	4.6	–	0.2	0.30

Elements such as chromium, molybdenum, tungsten, niobium, rhenium, and tantalum have the properties of both solid solution strengtheners and active carbide formers (chromium, tantalum, tungsten), and they are preferentially distributed in the γ-solid solution. The introduction of these elements into the alloy of the considered type may be justified to ensure phase-thermal stability during engine operation, but this is possible only with a certain balance of tungsten, molybdenum and chromium content. When complex alloying with refractory metals, it is important to take into account their liquidation coefficients, especially when forming alloys with an oriented structure. The introduction into the composition of the alloy of elements that increase the difference in density between the main melt and the liquat (such as Al, Ti, Nb, and others), as well as refractory elements (W, Re, Mo, and others), can contribute to the formation of surface defects of liquation origin during process of directional crystallization, especially at low crystallization rates.

The heat-resistant corrosion-resistant nickel-based alloy CM88Y [9] (**Table 4.5**) with a long-term strength of 280 MPa (900 °C, 100 h) was taken as the object of research. The purity of the alloy in terms of the content of harmful impurities must meet the requirements of the AMC 2280 standard. This alloy is used to make the working blades of the 1st and 2nd stage GTE turbines.

The alloying complex of SM88Y type alloys was optimized by adding to it the refractory elements of rhenium and tantalum as promising for additional alloying. These elements contribute to the strengthening of the austenitic solution, increase the structural stability of the alloy as a whole by reducing the diffusion mobility of the elements in the alloy, especially at high temperatures, significantly strengthening the solid solution and stabilizing the strengthening γ'-phase. Taking into account the results of our own experiments and literature data, it was established that alloying heat-resistant alloys with elements that have large atomic radii, such as rhenium and tantalum, is justified. These elements, with atomic radii exceeding the radius of nickel (the ratio for rhenium is 1.063), have a positive effect on the correspondence of crystal lattice periods in the γ-solid solution and the strengthening γ'-phase, which leads to an increase in the long-term strength of alloys at high temperatures. Rhenium also inhibits the processes of coagulation of the γ'-phase in the structure of the alloy and helps increase its thermal stability.

During the selection of the optimal metal alloying method and the study of the effect of individual elements on the structure and properties of the castings, the optimal chemical composition of the alloy was analyzed using linear regression analysis and taking into account the predicted structural stability of the alloy, which was determined by the PHACOMP program [21]. This method is based on the calculation of the possibility of the formation of the σ-phase in the γ-solid solution of complex heat-resistant alloys. The intensity of σ-phase formation depends on the number of electron vacancies Nv in the alloy matrix, excluding those that form carbides and borides in the alloy.

To determine the concentration of electron vacancies, it is necessary to establish the sequence of formation of phases in alloys and the sequence of their formation in the γ-matrix. This sequence includes the following stages: first, the formation of borides $(Mo_{0.5}Ti_{0.15}Cr_{0.25}Ni_{0.1})_3B_2$ occurs, then the formation of carbides occurs, in particular mono carbides ZrC, HfC, TaC, NbC, TiC and complex carbides Me_6C, $Me_{23}C_6$ and the formation of strengthening γ'-phase $(Ni_{0.88}Co_{0.08}Cr_{0.04})_3$ (Al, Ti, Ta, Nb, Hf, V). After studying these reactions, the composition of the residual matrix can be established, which allows to calculate the number of electron vacancies $N_{v\ av}$. According to the calculations, the N_v of the experimental alloy with the addition of rhenium and tantalum is 2.3, and that of the SM88Y alloy is 2.35. According to literature data, this indicator should not exceed 2.4 [22].

The obtained values of the coefficients in the regression equations (**Table 4.6**) showed that chromium has the greatest influence on the mass loss (Lg Metal loss), with an increase in chromium, the corrosion properties of the alloy increase. Rhenium also has a positive effect on the corrosion properties of the experimental alloy. Rhenium and titanium have a positive effect on the amount of the strengthening γ'-phase, when their content in the alloy increases, the volume of the γ'-phase increases (**Table 4.7**). Alloying heat-resistant alloys with rhenium and tantalum allows to increase the heat resistance of the cast metal (**Table 4.7**). This is achieved by increasing the amount of dispersed γ'-phase and strengthening the γ-phase due to cobalt, chromium, molybdenum, tungsten and rhenium. Even with a chromium content of 12.75 % by mass, the corrosion resistance of the experimental alloy remains at the level of the SM88Y alloy.

Table 4.6 Results of calculations of the composition of the experimental alloy with the addition of rhenium and tantalum using linear regression analysis

Alloy index	**Regression equation**
Corrosion resistance: Lg Metal loss (mass loss index)	$1.47437-0.602207\times C-0.146826\times Cr+0.0201633\times Ti-0.293672\times Re$ $R^2=99.985\ \%$
Lg corros Rate (corrosion rate indicator)	$1.52-0.0376815\times Cr-0.219755\times Ti-0.185562\times Re$ $R^2=97.9276\ \%$
The number of γ', at. %	$16.7844-39.5125\times C+9.47215\times Ti+3.33362\times Re$ $R^2=99.1566\ \%$

Table 4.7 Characteristics of experimental alloys

Alloy brand	**The volume of the γ'-phase in the alloy structure, %**	**Dissolution temperature of the γ'-phase, °C**	**Liquidus temperature, T_L, °C**	**Solidus temperature, T_S, °C**	**Long-term strength of the alloy at 900 °C for 100 hours, MPa**	**Corrosion resistance according to the mass loss index LgMetalloss**	**Corrosion rate in depth, LgcorrosRate**
Experimental alloy	44.8	1170	1385	1320	330	–1.611	–0.161
CM88Y	43.2	1180	1320	1270	275	–1.372	0.115

According to the calculations, the optimal content of the experimental alloy with the limit alloying with refractory metals was determined by mass %: Ni base; (0.04–0.07) C; (12.3–13.2) Cr; (3.0–3.5) Al; (1.8–2.3) Those; (6.8–7.5) So; (0.03–0.05) Zr; (0.45–0.50) Fe; (0.9–1.4) Mo; (6.0–6.6) W; (0.1–0.5) Nb; (2.5–4.3) Yes; (3.7–4.3) Re [23]. Samples of the above composition were melted by vacuum-induction melting, and for comparative studies of the SM88Y alloy, the temperature of pouring the melt into molds was 1560–1580 °C, the temperature of the mold was 800 °C.

Studies of the microstructure of the samples in the as-cast state confirm that the phase-structural state corresponds to the characteristics of the alloy of the considered type, and includes a γ-solid solution with the presence of the γ'-phase and carbides. **Fig. 4.8** clearly illustrates the microstructures of samples of heat-resistant alloy SM88Y and the experimental alloy.

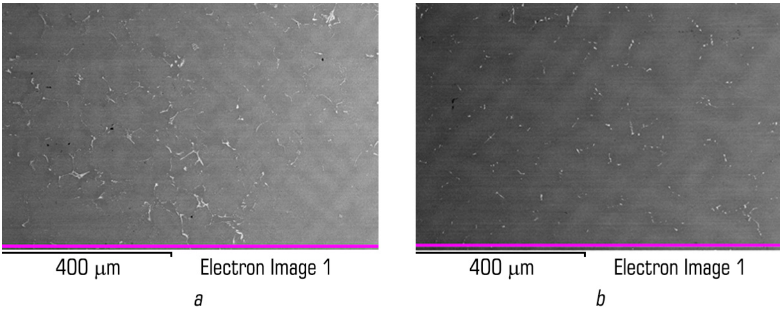

a *b*

Fig. 4.8 Microstructure of samples of heat-resistant alloys in the cast state: *a* – CM88Y; *b* – experimental alloy

With the help of a high-precision synchronous thermal analyzer STA 449F1 of the company "NETZSCH" (Germany), the temperatures of phase transitions in the experimental alloys were determined using a specially developed method. The addition of rhenium and tantalum to the alloy resulted in an upward shift of the solidus (T_S) and liquidus (T_L) temperatures to approximately 1320 °C and 1385 °C, respectively, compared to values of 1270 °C and 1320 °C without these additions elements, which makes it possible to raise the operating temperature of turbine blades by more than 50 °C compared to the SM88Y alloy. In addition, the dissolution temperature of the strengthening intermetallic γ'-phase of the experimental alloy remains at the level of the SM88Y alloy (**Table 4.7**).

Based on the obtained temperatures of phase transitions, the heat treatment mode was set: 1220 °C, 4 h+1050 °C, 4 h+870 °C, 20 h, cooling after each stage of heat treatment in air [24]. The results of tests on short-term strength showed that the level of mechanical properties of all samples of the experimental alloy meets the requirements of the technical documentation for this product (**Table 4.8**).

The study of resistance to high-temperature salt corrosion of experimental alloys was carried out on cylindrical samples with a diameter of 8 mm in a salt solution of 25 % NaCl+75 % Na_2SO_4 (density 2.5 g/cm^3) for 30 hours. Corrosion indicators were determined by measuring mass loss and conducting metallographic studies, including analysis of the depth of corrosion in the metal (**Table 4.9**) [25–27].

Table 4.8 Mechanical properties of samples of experimental alloys

Test temperature, °C	Alloy	σ_B, MPa	$\sigma_{0.2}$, MPa	δ, %	ψ, %
20	CM88Y	1173	880	16.0	12.0
	Exp. alloy	1212	912	12.0	10.5
600	CM88Y	942	745	8.8	12.7
	Exp. alloy	1005	706	16.0	17.8
900	CM88Y	879	683	24.0	42.2
	Exp. alloy	880	673	19.2	42.2

Table 4.9 Corrosion indicators of experimental alloys

Alloy	Sample No.	Specific mass loss, mg/cm^2	Corrosion rate, mg/cm^2/h	Depth of external corrosion, mm	Depth of internal corrosion, mm
CM88Y	1	35.26	1.175	0.05	0.12–0.15
	2	28.85	0.962	0.24	0.10–0.12
Experimental	3	28.70	5.896	0.28	0.05–0.10
	4	27.82	9.627	0.05	0.05–0.10

The conducted set of studies showed that the increase in the volume fraction of the strengthening γ'-phase is achieved due to the optimal combination of such elements as aluminum (Al), titanium (Ti) and tantalum (Ta). After the introduction of rhenium and tantalum into the alloy, an increase in the dissolution temperature of the γ'-phase is noted, which has a positive effect on its heat resistance. Phase stability and strengthening of the γ-solid solution is ensured by alloying with refractory elements, such as tungsten (W), molybdenum (Mo) and rhenium (Re). In addition, the optimal combination of alloying elements has been established in order to minimize the probability of formation of topologically densely packed phases in castings of heat-resistant corrosion-resistant alloys for gas turbine blades. Reducing the chromium (Cr) content in the experimental alloy ensures its corrosion resistance. Optimization of the content of carbon (C), boron (B), zirconium (Zr), hafnium (Hf) and yttrium (Y) was performed in order to improve the quality and durability of the alloys.

4.3 THE INFLUENCE OF EXCESS PRESSURE ON THE PROPERTIES AND QUALITY OF CASTINGS FROM IRON-CARBON ALLOYS WHEN LOST FOAM CASTING

4.3.1 FEATURES OF THERMAL DESTRUCTION OF POLYSTYRENE UNDER THE ACTION OF EXCESS PRESSURE

The phase composition and ratio of thermal destruction products of the model plays a major role in shaping the quality of castings obtained by casting on gasified models. It was established that when filling the form with metal, the model material undergoes all the main stages of transformation when heated – melting, evaporation, partial oxidation and gasification with the formation of liquid, solid and gaseous phases [28]. At the same time, the effect of high pressure created in the "metal – model" system on the conditions of thermal destruction of polystyrene foam has not been studied.

To study the processes of destruction of the polystyrene pattern under the conditions of metal pouring under excessive pressure, a special technique and equipment were developed, which are schematically presented in **Fig. 4.9**.

The unit includes a steel sleeve 1, in which the investigated polystyrene sample 2 is placed and a metal mesh 3, which is designed to prevent metal from entering the pipeline 4, which removes destruction products from the sleeve, trap 5 for trapping the vapor-liquid phase, cylinder 6 for trapping the gaseous phase with a known volume, gas pressure sensor 7, which is connected to the automatic control system (ACS). The installation kit also includes a foundry container 8 with refractory filler 9, a ceramic riser 10, a punch 11 and a pressing chamber 12 with a case 13, into which liquid metal 14 is poured.

Fig. 4.9, *b* shows the assembled sleeve. For research, a sample with dimensions ∅50×50 mm, weight 2.5±0.2 g, which corresponds to the density of the model $\rho_5 = 25–26$ kg/m^3, was selected.

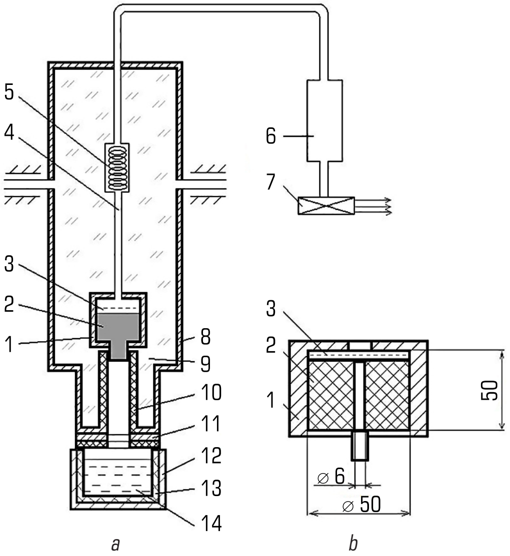

Fig. 4.9 Scheme of the unit (*a*) and sleeve (*b*) for studying thermal destruction of polystyrene when high pressure is applied to the metal

A central hole ∅6 mm is provided in the center of the sample for the release of destruction products during pyrolysis. The sample is installed in the sleeve at a height of 10 mm from the bottom edge so that decomposition products do not enter the mold cavity at the moment of contact of the sample with the metal. A layer of non-stick, non-gas-forming coating is applied to the inner surface of the sleeve, which is dried at a temperature of 230–250 °C for 1.5–2.0 hours.

After installing the sample, the nozzles for the release of decomposition products from the sleeve are hermetically connected by a pipeline 4 to the trap 5, which is filled with glass wool, where part of the vaporous decomposition products condenses at room temperature.

Another part of the solid destruction products settles on the inner surface of the sleeve above the sample. After the trap, the gaseous decomposition products enter cylinder 6 through a sealed pipeline. The temperature of the gas in the cylinder is measured by a thermoelectric sensor. At the moment of contact of the sample with liquid metal, its decomposition begins. The release of gaseous products leads to an increase in the pressure in the system, which is perceived by the pressure sensor 7 and controlled by the ASC.

The volume of gas released during sample decomposition was calculated according to formula (4.1):

$$V = V_0' - V_0, \tag{4.1}$$

where V_0' – the total volume of air in the system brought to normal conditions and released during gas decomposition, m^3; V_0 – the volume of the system brought to normal conditions, m^3.

The amount of vapor phase (VP) condensed in the trap was determined as the difference between the mass of the trap before and after the experiment: G_1 and G_2, respectively, and the mass of soot products as the difference between the mass of the trap G_3 after removing the condensed liquid fractions by keeping the trap at 200 °C and by the mass of the trap to experiment G_1.

The mass of the resulting gas mixture (GM) was determined by the known density (ρ=0.67 kg/m^3) and the experimentally determined volume.

The thermal destruction conditions of the polystyrene pattern of the real shape were determined in the temperature range of 1050–1520 °C by filling the mold with GM carbon steel (T=1520 °C) and cast iron (T=1300–1450 °C). During the implementation of this series of experiments, the metal lifting speed varied in the range of 25–150 mm/s, and the constant parameters were the pressure on the liquid metal (P_m=0.5 MPa) and the density of the model (ρ_5=25.5±0.5 kg/m^3).

The analysis of the data on the thermal destruction of the model shows that an increase in the metal lifting speed from 25 to 150 mm/s leads to a decrease in the specific gasification rate of polystyrene a_5 by 2.4–3.2 times. At the same time, a change in the temperature of the melt within one value of the speed W_1 has no significant effect on the change in the value of a_5. In this case, the deviation of the value of a_5 from the average does not exceed 5÷10 %. This allows to determine the kinetics of the change in the value of Q_5 as an average $\bar{Q}_5$ for each value of the rate of rise of the metal in the form of W_1. In this case, the kinetics of the change in the gasification coefficient Q_5 can be imagined as a dependence $y = A \cdot X^B$ that determines the functional relationship between the time of filling the mold with the sample (X) and its gasification coefficient (Y).

To find the values of the coefficients A and B, mathematical data processing was used, which is based on the method of minimum errors, which made it possible to obtain the equation of the kinetics of thermal destruction of the polystyrene foam pattern in real form when pouring alloys in the temperature range of 1050–1520 °C, which has the form:

$$Q_5 = 58.5\sqrt{t_3},\ \text{cm}^3/\text{h}. \qquad (4.2)$$

Graphical interpretation of the gasification kinetics of the model on the basis of the data obtained according to equation (4.2) in the setting of full-scale experiments is presented in **Fig. 4.10**.

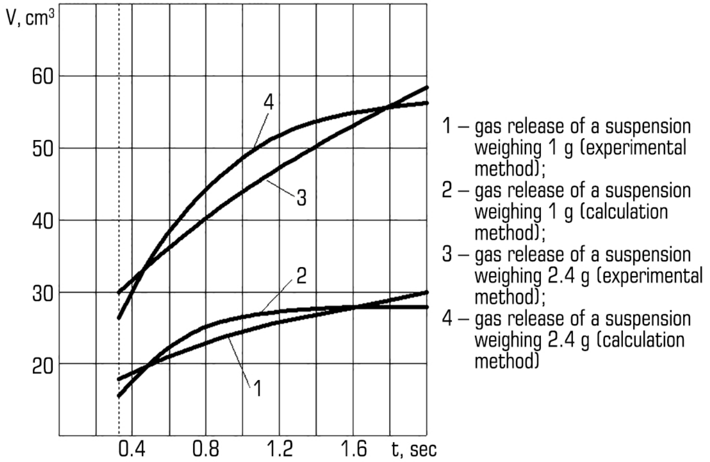

Fig. 4.10 Kinetics of gasification of a polystyrene model when pressure (P=0.5 MPa) is applied to the crystallizing liquid metal

When comparing the calculated (**Fig. 4.10**, curves 2, 4) and experimental (**Fig. 4.10**, curves 1, 3) curves describing the gasification kinetics of the model, a fairly high commonality between the calculated and experimental data was established. It was determined that the relative error between the data is within 2÷12.5 %. This allows to assert that experimental data and mathematical calculations can be used in the analysis of the conditions of thermal destruction of polystyrene foam in a form with the imposition of high pressure P_1, as well as in technological calculations for predicting the quality of cast blanks when lost foam casting, with the imposition of pressure on liquid and crystallising metal.

Generalized data on the number of gaseous, vapor-gas, and solid phases depending on the speed of metal ascent in the form of W are presented in **Table 4.10**.

When analyzing these data (**Table 4.10**), it was found that when the speed of W_1 increased from 25 to 150 mm/s, the amount of gaseous phase (GP) and solid phase (SP) decreased by 2.5 and 1.5 times, respectively, and the amount of vapor-gas phase (VGP) increases by 3.2 times (**Fig. 4.11**).

Table 4.10 Number of gaseous, vapor-liquid and solid phases during thermal destruction of a polystyrene foam sample weighing 2.4 g

Amount of phase, g, (%)	**Phase name**	**Metal lifting speed in the form of mm/s**					
		25	**50**	**75**	**100**	**125**	**150**
	Gaseous	0.160 (7)	0.114 (5)	0.094 (4)	0.08 (3.3)	0.072 (3.0)	0.066 (2.7)
	Vapor gas	0.32 (13)	0.701 (30)	0.818 (34)	0.906 (36.7)	0.976 (40)	1.004 (42.3)
	Solid	1.92 (80)	1.585 (65)	1.488 (62)	1.414 (60)	1.352 (57)	1.330 (55)

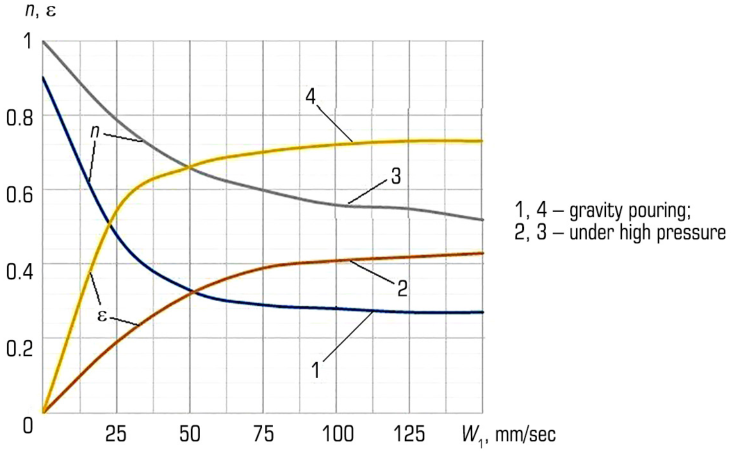

Fig. 4.11 The influence of the metal rising speed in a mold with a gasifying model on the degree of gasification (n) and the accumulation of the liquid phase (ε) during the casting of iron-carbon alloys under high pressure ($P > 0.5$ MPa)

This character of the change in the volume (mass) of GP, VGP differs from similar ones during the thermal destruction of GM during gravity casting (**Fig. 4.11**, curves 3, 4), which indicates a change in the mechanism of thermal destruction of polystyrene foam when pressure is applied to liquid metal and metal that crystallizes.

It is important, on the basis of the available data, to determine the gasification coefficient ε, liquid phase accumulation ξ as parameters used for mathematical prediction of the quality of castings obtained by the LGM process [29]. In this case, the coefficients n and ε depending on the rate of rise W, and the kinetics of their change are presented in **Fig. 4.11**.

The analysis of these data shows that with an increase in the speed of W_1, the degree of gasification increases from 0.2 to 0.45 (**Fig. 4.11**, curve 2), and the value of the coefficient e naturally decreases from 0.8 to 0.55 (**Fig. 4.11**, curve 1). This character of the change in n and ε during gravity filling, as well as their kinetics of change, is reversed (**Fig. 4.11**, sections 3, 4).

Further, on the basis of the obtained data, it is advisable to determine the gasification coefficients of the a_5 model, as a parameter used in the calculation of the volume, mass and degree of GM gasification.

To determine the relative coefficient a_5, let's use equation (4.2), but since the interaction between the metal and the Styrofoam model occurs in a plane perpendicular to the vector of the melt movement speed, it can be represented in the following form:

$$V_d = a_5 F_5 \sqrt{\tau},\ \text{cm}^3. \tag{4.3}$$

At the same time, the physical content of the introduced equation (4.3), the physical content of the coefficient a_5, which determines the amount of gas released from a unit of the interaction surface in the "metal – part" system per unit of time τ, should be clarified. In this case, if:

$a_5 F_a = 169.37$, and since $F = 19.34$ cm^2,

$a_5 = \dfrac{169.34}{19.34}$ and finally, $a_5 = 8.76$.

At the same time, the rate of gas evolution at the destruction temperature of the polystyrene pattern can be represented in the form of an equation:

$$\frac{dV}{d\tau} = \frac{a_5 F_5}{2\sqrt{F}}, \tag{4.4}$$

destruction of the V_M model in the form of an equation:

$$V_M = b_5 F_5 \sqrt{\tau}, \tag{4.5}$$

and since $\dfrac{V_M}{V_d} = \dfrac{b_5 F_5 \sqrt{\tau}}{a_5 F_5 \sqrt{\tau}}$, then the coefficients of destruction of the model:

$$b_5 = a\frac{V_M}{V_d} = \frac{8.76 \times 96t}{545} = 1.55,$$

where b_5 – the destruction coefficient of the model; 545 – the amount of gas formed during complete gasification of the model weighing 2.4 g.

In this case, the kinetics of gasification V_G of the V_M model during high-pressure GM casting for iron-carbon alloys in the range of 1050–1570 °C is described by an equation of the following form:

$$V_F = 8.76F_5\sqrt{\tau},\ \text{cm}^3; \tag{4.6}$$

$$V_M = 1.55F_5\sqrt{\tau},\ \text{cm}^3. \tag{4.7}$$

Therefore, the mass P_5 of the destroyed model at this moment in time is determined by the expression:

$$G_5 = 1.55\rho_5 F_5\sqrt{\tau}. \tag{4.8}$$

The amount of liquid phase at any moment of time is determined according to the equation:

$$G_b = G_5 - 8.76\rho_D F_5\sqrt{\tau},\ \text{g}. \tag{4.9}$$

Equations (4.8) and (4.9) will make it possible to predict the conditions for the LP appearance on the surface of the front of the metal flow and the casting, which solidifies when excess pressure is applied.

It should be especially noted that during the setting of a series of experiments and the analysis of the obtained data on the thermal destruction of the expanded polystyrene pattern during pressure casting of iron-carbon alloys, the nature of the kinetics of thermal destruction was established, which is significantly different from the similar one during gravity casting. These differences can be explained by another mechanism of thermal influence in the "metal – model" system, which is based on the following: firstly, when the pressure is increased, the inequality is fulfilled: $P_1 \gg P_P + \sigma_5$, and it cannot be realized during gravity casting, so as well as $P_M < P_P + \sigma_5$, when $W_5 > 50$ mm/s, ($P_M^{\max} < 0.08$ MPa), σ_5 – the thermomechanical resistance of GM, ($\sigma_5 \geq 0.15$ MPa); secondly, the filling of the form at $W_1 > 40$ mm/s leads to the formation of a new system of thermodynamic influence – "metal – vapour-gas gap – spheroids of the liquid phase – model". These initial conditions, which differ from gravity casting along GM, change the mechanism of thermodynamic interaction. When pouring the mold, the gap – "metal – model" is filled with a liquid phase, which under pressure P_1 is pressed into the mold and the heat flow from the melt to the model q_5 is transmitted through the LP with a thickness Δ, which is a thermal resistance and depends on the value of Δ. As the speed of W_1 increases, the thickness of the gap decreases and the thermal resistance decreases, which leads to an increase in the power of the heat flow q_5 and, therefore, the gasification rate of the polystyrene foam pattern increases. On the contrary, during gravity casting ($W_1 \leq 40$ mm/s), a "metal-model" gap is first formed, and the surface of the flow front is partially covered by LP. In this case, the heat transfer from the melt to the model is mainly transmitted by radiant energy, where $q_T = f\left(T_4\right)$, which explains that during gravity casting, the degree of gasification of polystyrene foam is higher than during pressure casting and significantly depends on the temperature of the metal being poured T_1, which is not observed during pressure casting.

Thus, on the basis of the conducted research, the mechanism of heat-force interaction of the metal with the polystyrene foam pattern, the conditions, the kinetics of its gasification depending on the casting parameters were established, and a mathematical apparatus was created that allows predicting the formation of defects in the casting caused by the interaction of the metal with the GM and determining the optimal parameters of GM casting under high pressure.

4.3.2 THE INFLUENCE OF TECHNOLOGICAL PARAMETERS OF LOST FOAM CASTING UNDER REGULATED PRESSURE ON THE PHYSICAL AND MECHANICAL CHARACTERISTICS OF CAST STRUCTURES MADE OF IRON-CARBON ALLOYS

It is known that applying pressure to the metal at the time of its hardening contributes to the formation of a denser structure in castings and reduces porosity [29, 30].

Research on the influence of casting parameters, in particular high pressure, on the physical and mechanical properties of castings was carried out on objects in the form of iron-carbon alloys – carbon and stainless steel, cast iron with spherical and vermicular graphite.

In order to study the thermodynamic influence on the development of the crystallization processes of the formation of castings during GM casting, a methodology was developed and special equipment was created, the scheme of which is presented in **Fig. 4.12**, and the levels of variation by variable factors are in the **Table 4.11**.

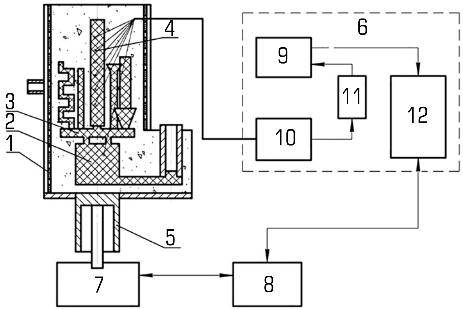

1 – experimental container;
2 – pressing chamber;
3 – pattern assembly of complex test;
4 – pressure sensors, thermal EMF, sensors of discrete signals;
5 – pressing piston;
6 – automated control system;
7 – drive;
8 – automated control system;
9 – controller;
10 – control sensors;
11 – converter;
12 – automatic adjustment system

Fig. 4.12 Scheme of the equipment for researching the influence of the main technological factors on the gas-hydrodynamic features, technical and technological properties of metal castings when lost foam casting, under excess adjustable pressure

Table 4.11 Experiment planning matrix

Factors	**Experiment No.**															
	1	**2**	**3**	**4**	**5**	**6**	**7**	**8**	**9**	**10**	**11**	**12**	**13**	**14**	**15**	**16**
Pressure P_1, MPa	3	6	3	6	3	6	3	6	3	6	3	6	3	6	3	6
Overheating, θ_1	1.25	1.25	1.05	1.05	1.25	1.25	1.05	1.05	1.25	1.25	1.05	1.05	1.25	1.25	1.05	1.05
Speed W_1, mm/s	80	80	80	80	20	20	20	20	80	80	80	80	20	20	20	20
Model density ρ_5, kg/m^3	50	50	50	50	50	50	50	50	20	20	20	20	20	20	20	20

As a result of mathematical processing of research data, performed in accordance with the experiment planning matrix (**Table 4.11**) with the application of the application program package, coefficients and regression equations were determined for each of the responses in the following form:

1. For carbon steel (Steel 45L):

a) strength limit σ_B, MPa:

$$Y = 35.1 + 5.68X_{16} + 24.3X_{17} - 0.103X_{18} - 0.226X_{19} - \\ - 4.536X'_6 + 0.0248X'_7 + 0.0446X'_8, \qquad (4.10)$$

where $X'_6 = X_{16}X_{17}$, $X'_7 = X_{16}X_{18}$, $X'_8 = X_{16}X_{19}$;

b) porosity, P, %:

$$Y = -7.10 + 1.336X_{16} + 7.18X_{17} + 0.1193X_{18} - 0.01067X_{19} - 1.316X'_6 - \\ - 0.0216X'_7 + 0.00348X'_8 - 0.1059X'_9 + 0.00553X'_{10} - 0.0000574X'_{11} + \\ + 0.1937X'_{12} - 0.001619X'_{13}, \qquad (4.11)$$

where $X'_9 = X_{17}X_{18}$, $X'_{10} = X_{17}X_{19}$, $X'_{11} = X_{18}X_{19}$, $X'_{12} = X'_{11}X_{17}X_{18}$, $X'_{13} = X_{16}X_{17}X_{19}$;

c) shrinkage ε, %:

$$Y = 4.18 + 1.493X_{19} + 5.555X_{17} + 0.09X_{18} - 0.0006X_{19} + +0.348X'_6 - 0.0213X'_7 + \\ + 0.000252X'_9 + 0.00638X'_{10} + 0.000049X'_{11} + 0.0182X'_{12}. \qquad (4.12)$$

2. For high-alloy steel (type Х18Н10ТЛ):

a) strength limit σ_B, MPa:

$$Y = 78.5 + 1.182X_{16} - 18.32X_{17} - 0.346X_{18} - 0.0499X_{19} - 0.879X'_6 + 0.0138X'_7 + \\ + 0.001239X'_8 + 0.287X'_9; \qquad (4.13)$$

b) porosity, P, %:

$$\begin{aligned}Y = {} & 2.80+0.655X_{16}+3.238X_{17}+0.0563X_{18}-0.0253X_{19}-0.695X'_{6}-\\ & -0.00499X'_{7}-0.0015X'_{8}-0.05122X'_{9}+0.0175X'_{10}-\\ & -0.000499X'_{11}+0.00928X'_{12};\end{aligned}\tag{4.14}$$

c) shrinkage ε, %:

$$\begin{aligned}Y = {} & -2.44+0.971X_{16}+4.15X_{17}+0.0662X_{18}-0.0088X_{19}-\\ & -0.907X'_{6}-0.013X'_{7}+0.000X'_{8}-0.057X'_{9}+\\ & +0.0126X'_{10}-0.0115X'_{12}.\end{aligned}\tag{4.15}$$

3. For cast iron with spherical graphite:

a) strength limit σ_B, MPa:

$$\begin{aligned}Y = {} & 154-3.483X_{16}-96.65X_{17}-0.184X_{18}-1.84X_{19}+3.608X'_{6}+0.0048X'_{7}+\\ & +0.01954X'_{8}+0.186X'_{9}+1.45X'_{10}+0.0004737X'_{11};\end{aligned}\tag{4.16}$$

b) shrinkage ε, %:

$$\begin{aligned}Y = {} & 1.66-0.1349X_{16}-0.2867X_{17}-0.00455X_{18}+0.0003753X_{19}+0.029X'_{6}+\\ & +0.00055X'_{7}+0.000374X'_{8};\end{aligned}\tag{4.17}$$

c) porosity, P, %:

$$\begin{aligned}Y = {} & -0.984+0.2352X_{16}+1.365X_{17}+0.017X_{18}-0.00428X_{19}-0.2647X'_{6}-\\ & -0.00347X'_{7}+0.0008337X'_{8}-0.01689X'_{9}+0.333X'_{10}.\end{aligned}\tag{4.18}$$

4. For cast iron with lamellar graphite:

a) strength limit σ_B, MPa:

$$\begin{aligned}Y = {} & 61.4-1.479X_{16}-22.59X_{17}-0.0894X_{18}-0.6204X_{19}+1.118X'_{6}+\\ & +0.0145X'_{7}-0.002098X'_{8}+0.002239X'_{9}+0.4301X'_{10}+0.001424X'_{11};\end{aligned}\tag{4.19}$$

b) shrinkage ε, %:

$$\begin{aligned}Y = {} & 1.72-0.1645X_{16}-0.2492X_{17}-0.004X_{18}-0.00125X_{19}+0.0207X'_{6}+\\ & +0.0005833X'_{7}+0.001042X'_{8}.\end{aligned}\tag{4.20}$$

The assessment of the adequacy of the obtained mathematical dependencies to the experimental data was carried out using the Fisher statistical test, and the significance of the regression coefficients was checked using the Student's t-test.

To assess the effect of pressure P_1 and the overheating degree θ_1 on the formation of the physical and mechanical properties of the metal of castings obtained by lost foam casting, it is advisable to use the graphical interpretation of the regression equation for σ_B, P_1, ε, which are presented in **Fig. 4.13–4.18**.

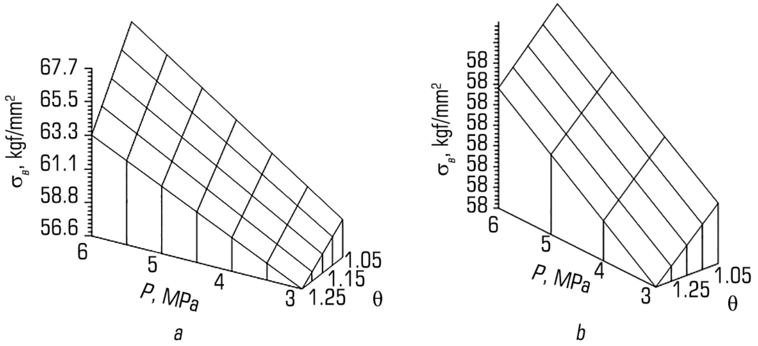

Fig. 4.13 Influence of pressure P_1 and the degree of metal overheating on the strength σ_B in: *a* – carbon steel; *b* – alloy steel

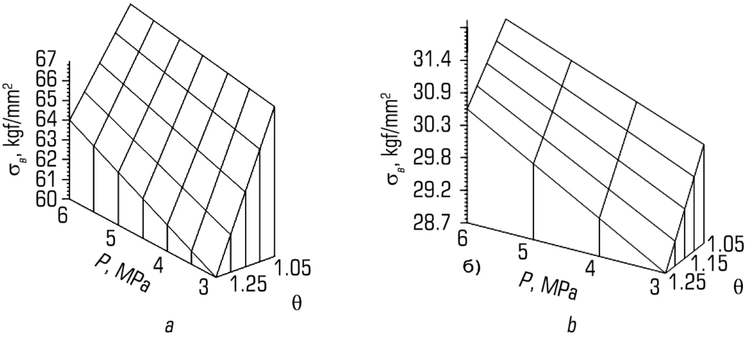

Fig. 4.14 Influence of pressure P_1 and the degree of metal overheating θ_1 on the strength σ_B of: *a* – high-strength cast iron; *b* – gray cast iron

Based on the analysis of these graphical data, it was established that an increase in pressure P_1 leads to an increase in the strength characteristics for all studied alloys. Moreover, the maximum increase in strength is achieved with minimal overheating of the melt θ_1. Thus, the increase in the value of σ_B for castings made of carbon and alloy steels, gray and high-strength cast iron amounted to 23 %, 17 %, 17 %, and 19 % (**Fig. 4.13, 4.14**), respectively.

At the same time, an increase in the degree of overheating from 1.05 to 1.25 reduces the value of pressure P_1 by σ_B and reduces these values compared to B_{max} by 10 %, 6 %, 9.6 %, and 4 %, respectively.

The nature of the effect of pressure P_1 and overheating σ_B^{max} on the kinetics of changes in porosity P_1 during casting of various alloys on GM is inversely related to their strength characteristics. Thus, increasing the pressure P_1 to a value of 6 MPa reduces the porosity in carbon, stainless steel castings by 3.75 and 2.35 times (**Fig. 4.15, 4.16**), respectively.

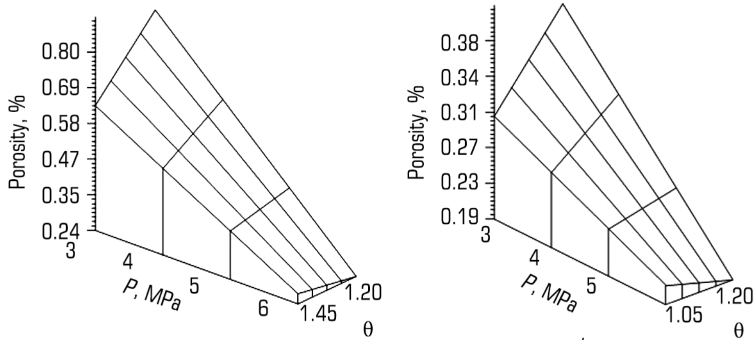

a *b*

Fig. 4.15 Influence of pressure P_1 and the degree of metal overheating on porosity P in castings made of: *a* – stainless (X18H10) steel; *b* – carbon steel

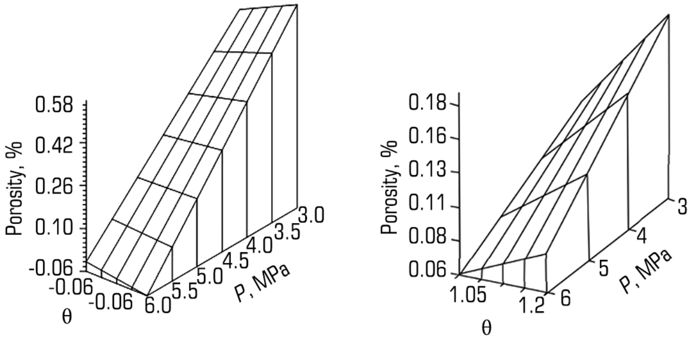

a *b*

Fig. 4.16 Influence of pressure P_1 and the degree of metal overheating θ_1 on the porosity of: *a* – high-strength cast iron; *b* – gray cast iron

Moreover, the maximum porosity P^{max} in castings made of carbon steel was 2 times higher than in castings made of stainless steel (**Fig. 4.15, *a*, *b***).

The influence of the degree of overheating in the melt at P^{max} and P^{max} on porosity is ambiguous. At a high level of pressure P^{max}, overheating practically does not affect the porosity, which changed only by 0.02 % and 0.03 %, respectively. At a low pressure P^{max}, the influence of the degree of overheating is significant. Thus, decreasing the value of θ_1 from 1.25 to 1.05 causes an increase in porosity in stainless steel and carbon steel castings by 0.3 and 0.12 %, respectively (**Fig. 4.15**).

A similar effect on the kinetics of porosity change with increasing pressure P_1 is observed in high-strength and gray cast iron castings (**Fig. 4.16**). Thus, increasing P_1 to a value of 6 MPa leads to a decrease in porosity in high-strength and gray cast iron castings from 0.73 to 0.06 % and from 0.24 to 0.06 %, respectively.

It should be noted that porosity in high-strength cast iron castings at low and high pressure does not depend on the degree of overheating θ_1. On the contrary, the porosity in gray cast iron castings increases with increasing superheat θ_1, although its absolute values are lower than those of high-strength cast iron by a factor of 3.

The nature of the kinetics of changes in the linear shrinkage of carbon and stainless steels when pressure P_1 is applied is identical.

As the pressure P_1 increases to 6 MPa, the shrinkage of carbon and stainless steels decreases from 2.35 to 2.27 % and from 2.37 to 2.20 %, respectively (**Fig. 4.17**). Moreover, the absolute values of ε^{min} and ε^{max} for both types of steel are practically equal (**Fig. 4.17**).

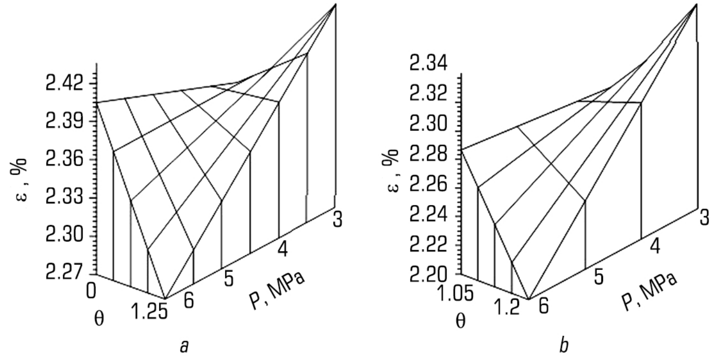

a *b*

Fig. 4.17 Influence of pressure P_1 and the degree of metal overheating θ_1 on the linear shrinkage of: *a* – carbon (Steel 45L) steel; *b* – alloy (X18H10) steel

Overheating of alloys above T_s in the studied temperature range also insignificantly changes the value of ε, although this value is more typical for carbon steels.

The influence of P_1 on the kinetics of change in casting shrinkage of cast iron with spherical and lamellar graphite is more noticeable. Here, increasing the pressure P_1 from 3 to 6 MPa reduces the casting shrinkage for cast iron with compact graphite and plate-vermicular graphite by 1.6 and 2.3 times, respectively (**Fig. 4.18**).

Imposition of pressure P_1 on liquid metal and crystallizing metal, the value of which ($P_1 > 0.5$ MPa) significantly exceeds the metallostatic pressure H_1 during gravity casting by GM, where $H_1 < 0.08$ MPa. In connection with this, the conditions of thermal interaction in the "metal – form" system change. Firstly, during pressure casting, there is no "gap" δ for a long period after pouring, which significantly increases the heat transfer coefficient α – in the "metal – form" system compared to heat exchange in the "metal – thermal gap – form" system during gravity casting.

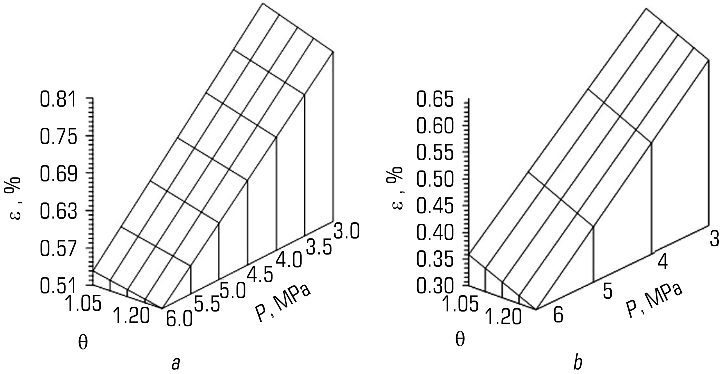

Fig. 4.18 Influence of pressure P_1 and the degree of metal overheating θ_1 on the linear shrinkage of: *a* – gray cast iron; *b* – high-strength cast iron

For example, with regard to the conditions of solidification of a casting made of carbon steel (Steel 45L), it was established that the influence of pressure P_1 on the liquid metal in the range of 3.0–6 MPa increases the rate of removal of overheating and crystallization of the metal in comparison with gravity casting, which is in the first 40 s 4.25–2.75 °C/s versus 1 °C/s (**Fig. 4.19**), respectively. At the same time, it should be noted that a decrease in pressure of less than 4.5 MPa leads to an equalization of the cooling rates of the casting. Thus, already 360 s after pouring, the integral coefficient of the cooling rate became equal and amounted to 1.81 °C/s, respectively.

When studying the influence of the P_1 value on the crystallization of gray iron castings, it was established that increasing the P_1 pressure increases the cooling rate of the casting, which was 1.0 °C/s for pressure casting and 0.7 °C/s for gravity casting (**Fig. 4.20**).

The influence of pressure on the amount of linear shrinkage e of iron-carbon alloys, the nature of the kinetics of change, which is the same for all studied alloys, is determined by the creation with the help of its "ideally rigid form" and the development of deformation processes in the initial stage of metal solidification, since in this period $P_1 > \sigma_B^T$, where σ_B^T is the strength limit casting at high temperatures. In addition, an undeformed "hard" shape creates conditions for compensation of shrinkage due to pre-shrinkage expansion of cast iron.

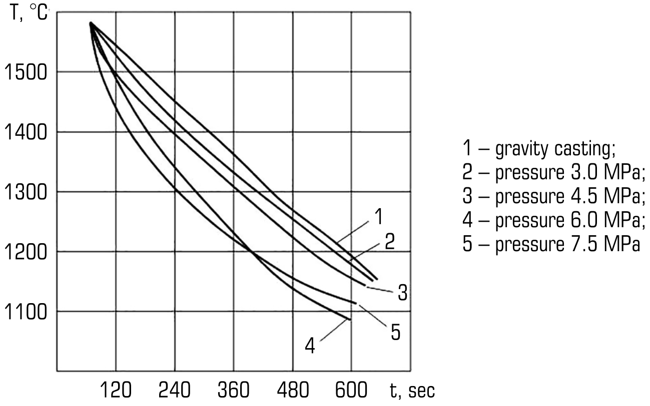

1 – gravity casting;
2 – pressure 3.0 MPa;
3 – pressure 4.5 MPa;
4 – pressure 6.0 MPa;
5 – pressure 7.5 MPa

Fig. 4.19 Carbon steel cooling curves depending on the amount of added pressure ($R_1 = 15$ mm)

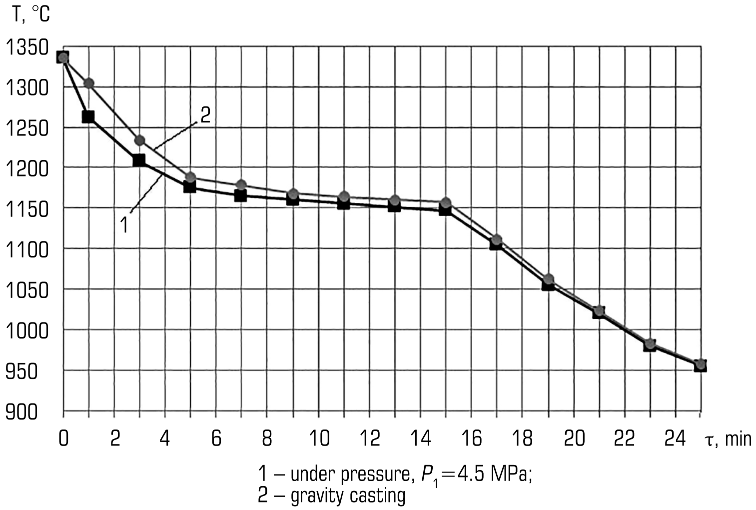

1 – under pressure, $P_1 = 4.5$ MPa;
2 – gravity casting

Fig. 4.20 Solidification kinetics of a cast iron casting ($R_1 = 15$ mm) during gravity casting and lost foam casting

Melt overheating θ in the investigated temperature ranges of the alloys being poured has a specific effect on the physical and mechanical properties of castings due to the intensification of heat removal during the pouring period. Thus, it was previously established [31] that additional removal of overheating due to losses due to thermal destruction of GM (30–50 °C for cast iron, 50–70 °C for steel) and an earlier transition to the liquid-solid and even solid-liquid state occurs, the latter possible only when applying high pressure. Thus, due to the removal of significant overheating and the presence of a solid phase of the metal in the initial stage of pouring, the characteristic effect of the value θ_1 on the physical and mechanical properties of castings from iron-carbon alloys is determined.

In conclusion, it should be especially noted that applying pressure to liquid metal and crystallizing metal allows to increase the strength characteristics of castings from iron-carbon alloys in comparison with gravity casting in hollow molds according to GM, including carbon and stainless steels, high-strength and gray cast iron by 10 and 15 %, 12 and 15 %, respectively.

4.3.3 TECHNOLOGICAL SCHEME OF OBTAINING REINFORCED CASTINGS BY LOST FOAM CASTING UNDER REGULATED PRESSURE

The implementation of this method of obtaining reinforced cast structures of various weights and dimensions using the method of casting into vacuum molds with a macro reinforcing phase of polystyrene foam pattern developed at the PTIMA of the National Academy of Sciences of Ukraine using regulated pressure. At the same time, it is also possible to use expanded polystyrene patterns with oriented porosity of various types – both in the form of bodies of rotation, conical and shaped parts of various and complex configurations.

There are two options for implementing the introduction of heterogeneous elements into the body of the polystyrene pattern: mixing these materials into foamed polystyrene before sintering the pattern, and also by introducing reinforcing elements into a previously prepared cavity in the body of the polystyrene pattern [32].

The technological scheme of obtaining reinforced castings by filling a vacuum mold with a macro-reinforcing phase, which is placed in a gasifying model under excess external pressure, is presented in **Fig. 4.21**.

After the production of the model block, the operation of forming it into a foundry container with sand filler is carried out. Next, the container is installed on the filling of the "RODAST" unit with the help of a movable traverse. Lifting of the mold and edging of the casting container is carried out. The container is vacuumed to a vacuum of 0.07...0.08 MPa. Next, liquid metal is poured into the mold, after which the press piston is raised at a speed set by the controller, which depends on the type, configuration, and thermophysical characteristics of the reinforced system. Pressing is carried out under a pressure of 0.5...20 MPa. After the pressing is finished, the press piston is disconnected from the container and the press residue is separated. After that, the auxiliary hopper is connected, the forming mixture is removed. Castings are sent for punching, cutting and cleaning, and molding sand for thermal regeneration.

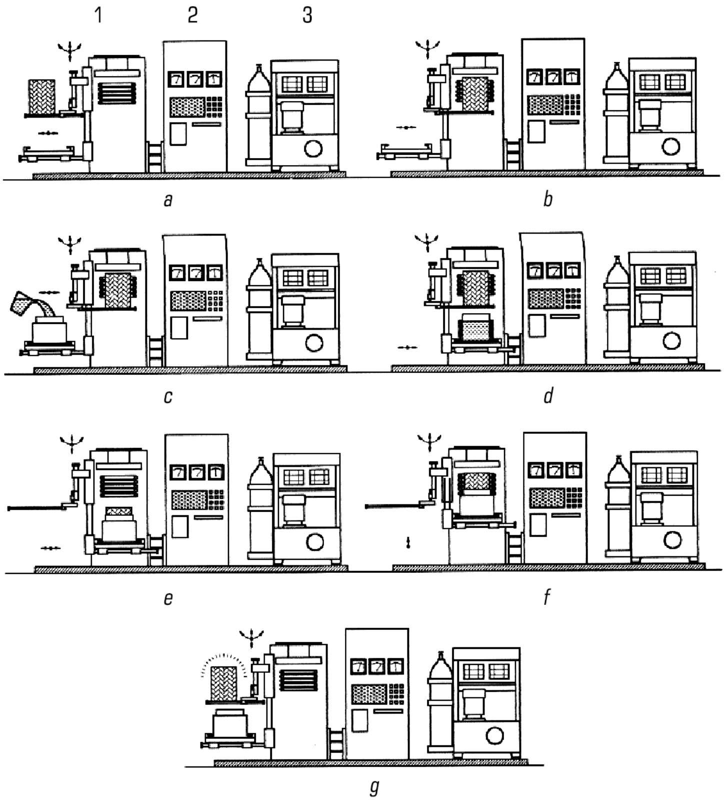

1 – RODAST – 10M1 unit; 2 – thyristor converter; 3 – hydrostation

Fig. 4.21 Technological scheme of obtaining LAM castings using external pressure: *a* – mold installation on the movable traverse; *b* – heating of the mold; *c* – pouring of the matrix alloy (MCA into the receiving bowl); *d* – transfer of the bowl from the MA to the pouring position; *e* – setting of the mold to the pouring position; *f* – filling of the form and LAM solidification under pressure; *g* – cooling the mold and removing the bowl

Thus, the main technological schemes for obtaining cast reinforced structures from iron-carbon alloys, which can be used for non-ferrous alloys, have been created. The main technological schemes created make it possible to obtain reinforced structures that work in extreme and normal conditions.

CONCLUSIONS

After vacuuming in the MHD mixer of liquid metal, which is stirred by electromagnetic forces, in continuously cast ingots from high-strength aluminum alloys, the hydrogen content decreases to 0.03...0.07 cm^3/100 g of metal, the concentration of oxide inclusions – to 0.04 vol. % and the solubility of alloying and modifying elements introduced into the melt increases.

In the production of continuously cast ingots from aluminum alloys, which contain easily oxidizable elements (Mg, Zn, etc.), it is necessary to create a protective environment of inert gases at all technological operations from melting to metal pouring. It is shown that in ingots made of alloy 1545 with a magnesium content of 4.5 % by mass, which were protected from oxidation, the breaking strength is 30 %, and the relative elongation is 2.4 times greater than in products obtained without the formation of a protective medium over metal.

Electromagnetic stirring of the alloy in the crystallizer significantly affects the structure and properties of continuously cast ingots. The use of electromagnetic stirring in ingot production processes allows controlling the speed of metal movement in the crystallizer and aligning the crystallization front of the alloy. As a result, the anisotropy of the properties and internal stresses in the ingots decreases, the nucleation process in the liquid metal intensifies, and the alloy structure is crushed. Thus, the ingots obtained without electromagnetic stirring of the B96C alloy in the crystallizer have a coarse crystal structure with a grain size of ~350 μm. In the ingots made from the alloy that was stirred, the structure is dispersed with a grain size of ~100 μm.

It is shown that after alloying the B93pch alloy with titanium in the amount of ~0.5 % by mass and subsequent plasma nitriding, a fine crystalline structure with the same grain size is formed in the ingots, which is 25–30 % smaller than in products made of non-nitrided metal. Complex MHD-plasma processing of the melt allows to increase the mechanical properties of pressed products from continuously cast ingots: the breaking strength and yield strength (σ_B, $\sigma_{0.2}$) increase by 7–10 %, relative elongation by 20–25 % compared to the requirements for stamped parts from alloy B93pch.

The above research results showed the optimal combination of such alloying elements as aluminum (Al), titanium (Ti), tantalum (Ta), tungsten (W), molybdenum (Mo), chromium (Cr) and rhenium (Re), which made it possible obtain high heat resistance, ensure phase stability of the alloy and its corrosion resistance.

The simultaneous influence of technological factors and excess pressure on liquid metal and crystallizing metal allows to increase the mechanical strength and reduce the porosity of the material of castings from carbon, stainless steel, high-strength and gray cast iron by 15–30 %, compared to gravity casting of GM.

Mathematical dependencies have been obtained for determining the mechanical and technological properties of castings made of carbon, stainless steel, high-strength and gray iron in the presence of excess pressure on the liquid metal, which crystallizes, which allows optimizing the technological parameters to obtain castings with the necessary operational properties.

The latest technological processes for the production of reinforced castings by the method of lost foam casting, using excess pressure on the metal, have been developed.

CONFLICT OF INTEREST

The authors declare that they have no conflict of interest in relation to this research, whether financial, personal, authorship or otherwise, that could affect the research and its results presented in this paper.

REFERENCES

1. Polyvoda, S. L., Siryi, O. V., Hordynia, O. M., Puzhailo, L. P. (2017). Pat. No. 119406 UA. Plavylno – lyvarnyi kompleks dlia napivbezperervnoho lyttia zlyvkiv z aliuminiievykh splaviv. MPK B22D 11/14. No. u201703178; declareted: 03.04.2017; published: 25.09.2017, Bul. No. 18. Available at: https://uapatents.com/5-119406-plavilno-livarnijj-kompleks-dlya-napivbezperervnogo-littya-zlivkiv-z-alyuminiehvikh-splaviv.html
2. Puzhailo, L. P., Serii, A. V., Polivoda, S. L. (2010). Tekhnologiia i oborudovanie dlia polucheniia slitkov iz vysokoprochnykh aliuminievykh deformiruemykh splavov metodom polunepreryvnogo littia. Visnyk Donbaskoi derzhavnoi mashinobudivnoi akademii, 3 (20), 227–229. Available at: http://www.dgma.donetsk.ua/science_public/ddma/2010-3-20/article/10PLDMSL.pdf
3. Polyvoda, S. L., Siryi, O. V., Puzhailo, L. P. (2012). Pat. No. 100231 UA. Apparatus for manufacturing and electromagnet casting alloys into casting molds. MPK B22D 39/00, B22D 35/00, H05B 6/02. No. a200907285. declareted: 10.07.2009; published: 10.12.2012, Bul. No. 23. Available at: https://uapatents.com/4-100231-ustanovka-dlya-prigotuvannya-ta-elektromagnitnogo-rozlivannya-splaviv-u-livarni-formi.html
4. Puzhailo, L. P., Polyvoda, S. L., Siryi, O. V., Hordynia, O. M. (2019). Pat. No. 131179 UA. Sposib pryhotuvannia aliuminiievykh lihatur u mahnitohidrodynamichnykh ustanovkakh. MPK C22B 21/00. declareted: 15.06.2018; published: 25.09.2008, Bul. No. 1. Available at: https://base.uipv.org/searchINV/search.php?action=viewdetails&IdClaim=254473
5. Puzhailo, L. P., Gavriliuk, V. P., Polivoda, S. L., Seryi, A. V., Gordynia, A. N. (2012). Issledovanie protcessa polunepreryvnogo litia slitkov iz vtorichnogo aliuminievogo splava AD31. Metall i lite Ukrainy, 7, 20–22.
6. Polyvoda, S. L., Siryi, O. V., Puzhailo, L. P. (2013). Pat. No. 101343 UA. Method for producing high-strength aluminum wrought alloys containing zinc. MPK C22C 21/06, C22C 21/02, C22B 9/04, C22B 21/00. No. a201007359. declareted: 26.12.2011; published: 25.03.2013, Bul. No. 6. Available at: https://uapatents.com/5-101343-sposib-prigotuvannya-visokomicnikh-alyuminiehvikh-deformivnikh-splaviv-z-vmistom-cinku.html

7. Puzhailo, L. P., Siryi, O. V., Polyvoda, S. L. (2015). Pat. No. 108781 UA. Sposib rafinuvannia aliuminiievoho splavu u vakuumi. MPK C22B 21/00, C22B 9/04. No. a201310432. declareted: 27.08.2013; published: 10.06.2015, Bul. No. 11. Available at: https://uapatents.com/4-108781-sposib-rafinuvannya-alyuminiehvogo-splavu-u-vakuumi.html
8. Polyvoda, S. L., Polyvoda, M. O., Hordynia, O. M., Siryi, O. V., Puzhailo, L. P. (2017). Pat. No. 115590 UA. Sposib vyznachennia vmistu vodniu u ridkomu metali. MPK C22B 21/00, G01N 33/20, G01N 27/61, G01N 27/74. No. a201511064. declareted: 12.11.2015; published: 27.11.2017, Bul. No. 22. Available at: https://uapatents.com/6-115590-sposib-viznachennya-vmistu-vodnyu-u-ridkikh-alyuminiehvikh-splavakh.html
9. Puzhailo, L. P., Gavriliuk, V. P., Seryi, A. V., Polivoda, S. L., Gordynia, A. N. (2012). Modelirovanie magnitogidrodinamicheskikh protsessov elektromagnitnogo peremeshivaniia aliuminievogo splava v kristallizatore i teplovoi nasadke pri polunepreryvnom lite slitkov. Protsessy litia, 5, 54–60.
10. Narivskiy, A., Polyvoda, S., Voron, M., Siryi, O. (2022). MHD-processes and equipment for continuous casting of aluminum alloy ingots. Casting Processes, 4 (150), 22–27. doi: https://doi.org/10.15407/plit2022.04.022
11. Narivskyi, A. V., Shyriaieva, I. V., Hlike, A. P., Fedorov, V. V., Naidek, V. L. (2012). Pat. No. 98903 UA. Sposib rafinuvannia splaviv vid domishok. MPK C21C 7/10, C22B 9/04, C21C 7/072. No. a201108029. declareted: 25.06.2011; published: 25.06.2012, Bul. No. 12. Available at: https://uapatents.com/6-98903-sposib-rafinuvannya-splaviv-vid-domishok.html
12. Fikssen, V. M., Dubodielov, V. I., Naidek, V. L., Sychevskyi, A. A., Tunyk, V. O., Narivskyi, A. V., Hanzha, M. S. (2017). Pat. No. 113663. Sposib plazmovoi obrobky splaviv v mahnitodynamichnii ustanovtsi. MPK C22B 9/05, C21C 1/00, C21C 7/072, C22B 9/04, B22D 1/00. No. a201502163. declareted: 12.03.2015; published: 27.02.2017, Bul. No. 4. Available at: https://uapatents.com/6-113663-sposib-plazmovo-obrobki-splaviv-v-magnitodinamichnijj-ustanovci.html
13. Holländer, D., Kulawinski, D., Weidner, A., Thiele, M., Biermann, H., Gampe, U. (2016). Small-scale specimen testing for fatigue life assessment of service-exposed industrial gas turbine blades. International Journal of Fatigue, 92 (5), 262–271. doi: https://doi.org/10.1016/j.ijfatigue.2016.07.014
14. Balitskii, A. I., Kvasnitska, Y. H., Ivaskevich, L. M., Mialnitsa, H. P. (2018). Hydrogen and corrosion resistance of Ni-Co superalloys for gas turbine engines blades. Archives of Materials Science and Engineering, 1 (91), 5–14. doi: https://doi.org/10.5604/01.3001.0012.1380
15. Glotka, O. A., Olshanetskii, V. Yu. (2023). Mathematical Prediction of the Properties of Heat-Resistant Nickel Alloys After Directional Crystallization. Materials Science, 58 (5), 679–685. doi: https://doi.org/10.1007/s11003-023-00716-z
16. Wahl, J. B., Harris, K. (2016). CMSX-4 plus single alloy development, characterization and application development. Superalloys 2016: Proc. Of the 13th International Symposium on Superalloys. TMS, 25–33. doi: https://doi.org/10.1002/9781119075646.ch3

17. Cueto-Rodriguez, M. M., Avila-Davila, E. O., Lopez-Hirata, V. M., Saucedo-Muñoz, M. L., Palacios-Pineda, L. M., Trapaga-Martinez, L. G., Alvarado-Orozco, J. M. (2018). Numerical and Experimental Analyses of the Effect of Heat Treatments on the Phase Stability of Inconel 792. Advances in Materials Science and Engineering, 2018, 1–16. doi: https://doi.org/10.1155/2018/4535732
18. Kuznetsov, V. P., Lesnikov, V. P., Konakova, I. P., Popov, N. A., Kvasnitskaya, Yu. G. (2015). Structural and Phase Transformations in Single-Crystal Rhenium- and Ruthenium-Alloyed Nickel Alloy Under Testing For Long-Term Strength. Metal Science and Heat Treatment, 57 (7–8), 503–506. doi: https://doi.org/10.1007/s11041-015-9912-4
19. Wu, X., Makineni, S. K., Liebscher, C. H., Dehm, G., Rezaei Mianroodi, J., Shanthraj, P. et al. (2020). Unveiling the Re effect in Ni-based single crystal superalloys. Nature Communications, 11 (1). doi: https://doi.org/10.1038/s41467-019-14062-9
20. Klochykhin, V. V., Pedash, O. O., Danilov, S. M., Tyomkin, D. O., Naumyk, O. O., Naumyk, V. V. (2022). Hot Isostatic Pressing in the Manufacture of ZhS3DK-VI Alloy Turbine Blades with 50 % Returns in the Charge. Strength of Materials, 54 (6), 1043–1049. doi: https://doi.org/10.1007/s11223-023-00479-7
21. Zhang, J. S., Matsugi, K., Murata, Y., Morinaga, M., Yukawa, N. (1992). Evaluation of the phase stability of modified IN738LC alloys with New Phacomp. Journal of Materials Science Letters, 11 (8), 446–448. doi: https://doi.org/10.1007/bf00731099
22. Balyts'kyi, A. I., Kvasnyts'ka, Yu. H., Ivas'kevich, L. M., Myal'nitsa, H. P. (2018). Corrosion- and Hydrogen-Resistance of Heat-Resistant Blade Nickel-Cobalt Alloys. Materials Science, 54 (2), 230–239. doi: https://doi.org/10.1007/s11003-018-0178-z
23. Kvasnytska, Yu. H., Kliass, O. V., Kreshchenko, V. A., Mialnytsia, H. P., Maksiuta, I. I., Shynskyi, O. Y. (2016). Pat. No. 110529 UA. Zharomitsnyi koroziinostiikyi splav na nikelevii osnovi dlia lopatok hazoturbinnykh dvyhuniv. MKP C22C 19/05, C22C 19/00, C22C 19/03. No. a201401359. declareted: 12.02.2012; published: 12.01.2016, Bul. No. 1. Available at: https://base.uipv.org/searchINV/search.php?action=viewdetails&IdClaim=219233
24. Kvasnytska, Y. H., Ivaskevich, L. M., Balitskii, A. I., Kvasnytska, K. H., Mialnitsa, H. P. (2022). Structural and Mechanical Properties of the Nickel Alloy of Gas-Turbine Engine Blades. Materials Science, 57 (5), 688–694. doi: https://doi.org/10.1007/s11003-022-00596-9
25. Ivaskevich, L., Balitskii, A., Kvasnytska, I., Kvasnytska, K., Myalnitsa, H. (2022). Thermal Stability, Cyclic Durability and Hydrogen Resistance of Cast Nickel-Cobalt Alloys for Gas Turbine Blades. Advances in Mechanical and Power Engineering, 147–155. doi: https://doi.org/10.1007/978-3-031-18487-1_15
26. Kvasnytska, Yu. H., Ivaskevych, L. M., Balytskyi, O. I., Maksyuta, I. I., Myalnitsa, H. P. (2020). High-Temperature Salt Corrosion of a Heat-Resistant Nickel Alloy. Materials Science, 56 (3), 432–440. doi: https://doi.org/10.1007/s11003-020-00447-5
27. Balitskii, A. I., Kvasnytska, Y. H., Ivaskevych, L. M., Kvasnytska, K. H., Balitskii, O. A., Shalevska, I. A. et al. (2023). Hydrogen and Corrosion Resistance of Nickel Superalloys for

Gas Turbines, Engines Cooled Blades. Energies, 16 (3), 1154. doi: https://doi.org/10.3390/en16031154

28. Shinsky, O., Shalevska, I., Kaliuzhnyi, P., Shinsky, V., Lysenko, T., Shevchuk, T. et al. (2018). Principles of construction and identification of a multilevel system for monitoring parameters of technological cycle of casting. Eastern-European Journal of Enterprise Technologies, 5 (1 (95)), 25–32. doi: https://doi.org/10.15587/1729-4061.2018.141303
29. Niakan, A. A., Idris, M. H., Ourdjini, A., Karimian, M. (2012). Effect of Applying Air Pressure on Gas Porosity in Lost Foam Casting of Al-Si Alloy. Advanced Materials Research, 628, 150–155. doi: https://doi.org/10.4028/www.scientific.net/amr.628.150
30. Kaliuzhnyi, P. (2020). Influence of Sand Fluidization on Structure and Properties of Aluminum Lost Foam Casting. Archives of Foundry Engineering, 20 (1), 122–126. doi: https://doi.org/10.24425/afe.2020.131293
31. Shinsky, I., Shalevska, I., Musbah, J. (2015). Efficiency of influence of a metal macroreinforcing phase on process of solidification of large-sized castings. TEKA. Edition of Lublin University of technology, 15 (2), 51–59.
32. Kaliuzhnyi, P., Shalevska, I., Sliusarev, V. (2023). Microstructure of reinforced cast iron produced by lost foam casting. Archives of Metallurgy and Materials, 68 (4), 1369–1375. doi: https://doi.org/10.24425/amm.2023.146202